

# We are IntechOpen, the world's leading publisher of Open Access books Built by scientists, for scientists

**4,800**

Open access books available

**122,000**

International authors and editors

**135M**

Downloads

Our authors are among the

**154**

Countries delivered to

**TOP 1%**

most cited scientists

**12.2%**

Contributors from top 500 universities



**WEB OF SCIENCE™**

Selection of our books indexed in the Book Citation Index  
in Web of Science™ Core Collection (BKCI)

Interested in publishing with us?  
Contact [book.department@intechopen.com](mailto:book.department@intechopen.com)

Numbers displayed above are based on latest data collected.

For more information visit [www.intechopen.com](http://www.intechopen.com)



# The Dosimetry Calculation for Boron Neutron Capture Therapy

Li Deng, Chaobin Chen, Tao Ye and Gang Li

*Beijing Capture Tech Co., Ltd.*

*Institute of Applied Physics and Computational Mathematics*

*China*

## 1. Introduction

BNCT incorporates the targeting principles of chemotherapy and the anatomical localization principles of conventional radiotherapy but with three distinct advantages:

- Current boron compounds at the required concentrations are non-toxic.
- The time interval between drug administration and neutron irradiation can be chosen to maximize the concentration differential between tumour and normal tissue.
- Only the tissues located around the tumour volume are exposed to significant neutron activated boron damage.

Following the earliest suggestions that BNCT might be useful for the treatment of human cancers, interest developed regarding the application of BNCT to primary high-grade brain tumours – glioblastoma multiforme (GBM). It was postulated that the reduction of the blood brain barrier (BBB) in the vicinity of tumour could be exploited to selectively increase the concentration of boron in the brain tumour over normal brain. Initially sodium tetraborate (borax), was used as the vehicle for boron. Perhaps the early interest in applying BNCT to high-grade primary brain tumours stemmed from the fact that this was a cancer with a very poor prognosis. This would ensure that BNCT, even if minimally successful, would nevertheless appear superior to ineffective conventional therapies.

In addition to the considerations of beam quality, the beam should also be sufficiently intense to ensure that treatment times remain within reasonable limits. This facilitates the procedure for the patient and reduces the problem of patient motion during treatment. It should be realized that whereas conventional radiotherapy fractions are administered within a period of about 10 minutes, current clinical BNCT treatments often extend to a few hours per fraction (2001)<sup>[1]</sup>.

In order for BNCT to be successful, a sufficient amount of  $^{10}\text{B}$  must be selectively delivered to the tumor ( $\sim 20\mu\text{g/g}$  weight or  $\sim 10^9$  atoms/cell), and enough thermal neutrons must be absorbed by them to sustain a lethal  $^{10}\text{B}(n,\alpha)^7\text{Li}$  capture reaction. Since the high linear energy transfer (LET) particles have limited boron pathlengths in tissue (5-9 $\mu\text{m}$ ), the destructive effects of these high energy particles are limited to cells containing boron. Clinical interest in BNCT has focused primarily on the treatment of high grade gliomas, and either cutaneous primaries or cerebral metastases of melanoma, and most recently head, neck and liver cancer. Since BNCT is a biologically rather than physically targeted type of radiation treatment, the potential exists to destroy tumor cells dispersed in the

normal tissue parenchyma, if sufficient amounts of  $^{10}\text{B}$  and thermal neutrons are delivered to the target volume. At its simplest, this could be the two low molecular weight drugs borated phenylalanine (BPA) and containing polyhedral borane (BSH). However, the dose calculations become much more complicated when combinations of agents are used (2006)<sup>[2]</sup>.

Clinical dose distributions can be significantly influenced by tissue inhomogeneities. The accuracy of the transport geometry is a key factor to predict the dose distribution with Monte Carlo method. The distribution of mass densities and chemical compositions, which express the patient's anatomical structure, are needed for the precalculation of the physical cross sections before the dose calculation is done by making direct simulation of the interactions between the radiation and the patient's body. There are two types of computerized anthropomorphic phantoms that can be defined either by mathematical functions or by voxel-based volume arrays. The former is referred to the MIRD Phantoms (1978)<sup>[3]</sup>, the latter is always made from CT or MRI images and well known about Zubal Phantom (1994)<sup>[4]</sup> and Male Adult Voxel Phantom(2003)<sup>[5]</sup>. They both can be used to model the patients in internal or external radiotherapy. But in radiation treatment planning, phantoms, which are directly made from the patient's CT images, are essential for the prediction of dose distribution in patient's body. DeMarco *et al* (1998)<sup>[6]</sup> defined medias of air, lung, fat, water, muscle and bone to figure a patient's anatomical structure. WANG *et al* (2001)<sup>[7]</sup> treated voxels from the CT images above a user-specified electron density as bone and below as water. Ma *et al* (2002)<sup>[8]</sup> used air, tissue and bone to describe a human body. W Schneider(2000)<sup>[9]</sup>gave a recommendation of 24 materials for the CT images.

In 3D radiation treatment planning a patient model is commonly simulated by dividing it into voxels (cuboids), which have individual mass densities and chemical compositions. There are two kinds of work to do to establish a CT based voxel phantom from a patient's CT images. One is to set up the calibration of CT numbers to mass densities by fitting a set of CT numbers and mass densities of real tissues from ICRP (1975)<sup>[10]</sup> or ICRU-44 (1989)<sup>[11]</sup>. The other is to correlate the CT numbers with the elemental weights, which is usually done by defining several threshold values in order to classify the CT scale in Hounsfield unit (-1000~1500) into different groups and the elemental weights are then constant within each group.

In recent years, the importance of BNCT obviously increases. The relative researches have been done in America, Japan, Finland, Netherland, Argentina, China and Italy etc. Especial for Japan and Argentina, a large amount of clinical tests have been done and good effects have been achieved (1994, 2008)<sup>[12,13]</sup>. Development of treatment planning system (TPS) software is one of an important part of BNCT, where the physical dose calculation is a key. High precision and rapid computational time are the basic requirements for clinical trials.

This chapter, BNCT principle, TPS status, neutron beam, medical pro, post processor and dose calculation will be discussed.

## 2. BNCT principles

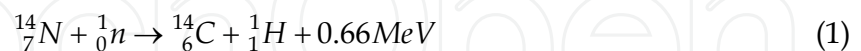
BNCT technique is used in treating brain tumors by artificially loading the tumor tissue with isotope Boron enriched compound and subsequently irradiation of brain by low energy neutrons. In recent ten years, BNCT has been used to treat the other tumors located at neck, liver and lung etc. The technique is based on the  $^{10}\text{B}(n,\alpha)^7\text{Li}$  nuclear reaction emitting alpha particle and  $^7\text{Li}$  nuclei with total kinetic energy of 2.79 MeV, which is high enough to destroy the tumor cells and avoids to hurt the normal tissue. A  $^{10}\text{B}$  nucleus absorbs a thermal

neutron and promptly emits a back to back  ${}^7\text{Li}$  ion and a  ${}^4\text{He}$  (alpha) particle. The combined range of 12–13  $\mu\text{m}$  is similar to mammalian cell dimensions.

### 2.1 Main nuclear reactions

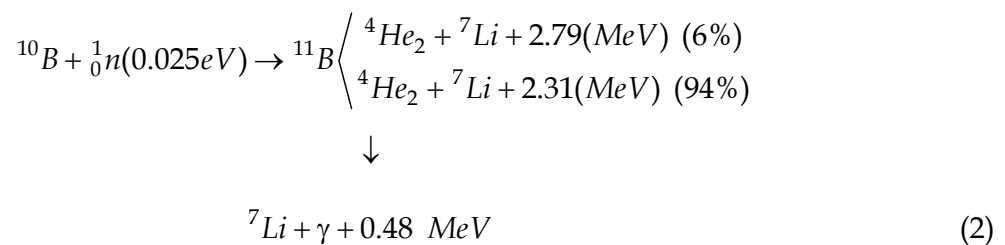
The doses are primarily from four parts: (1) thermal neutrons; (2) boron-10; (3) fast neutrons; and (4) photons. The relative nuclear reactions are given as following:

(1) Nitrogen capture reaction



Most of neutrons come from the thermal neutron in nuclear reaction. The release energy is deposited locally. The deposited dose is called as thermal neutron dose or proton dose. It is written by  $D_p$ .

(2) Boron neutron capture reaction



The release energy is deposited locally except for 0.48 MeV photon energy. The boron dose is written by  $D_B$ .

(3) Hydrogen capture gamma reaction



The photons are from hydrogen capture gamma reaction, boron neutron capture reaction and the neutron beam. The gamma energy is deposited step by step by Compton scattering and photoelectricity absorption. So the photon dose has a wide space distribution. The photon dose is written by  $D_\gamma$ .

(4) Elastic scattering of the fast neutron

The recoil protons are released when the elastic scattering is happened as soon as the epithermal and thermal neutron capture reaction with nitrogen. The proton energy is deposited locally. Of course, the energy of fast neutron is deposited by the elastic scattering, where 90% is from the nuclear reaction with nitrogen. The dose which is produced by the fast neutron elastic scattering is written by  $D_n$ . When the biological weighting factors are selected, the total biologically weighted dose, in Gy, becomes:

$$D_{bw} = w_c \cdot D_B + w_\gamma \cdot D_\gamma + w_n \cdot D_n + w_p \cdot D_p \quad (4)$$

Where  $D_{bw}$  is dose components,  $w_c$  is compound efficacy of the boron.  $w_\gamma$ ,  $w_n$ , and  $w_p$  are the relative biology efficacy of the photon, fast neutron and proton, respectively.

### 2.2 TPS status

TPS usually includes: (1) the medical pre-processor, i.e a 3-d model of patient's head, which is based on CT and MRI DICOM data, is created and then automatically produces a input

file of Monte Carlo code; (2) the dose calculation and (3) the post-processor, which plots the dose lines and surfaces of different tissues. Furthermore, the irradiation time and irradiation location are determined. Most of TPSs are developed from MCNP program [14]. Figure 1 shows a process of TPS. Figure 2 shows the flow of a TPS.

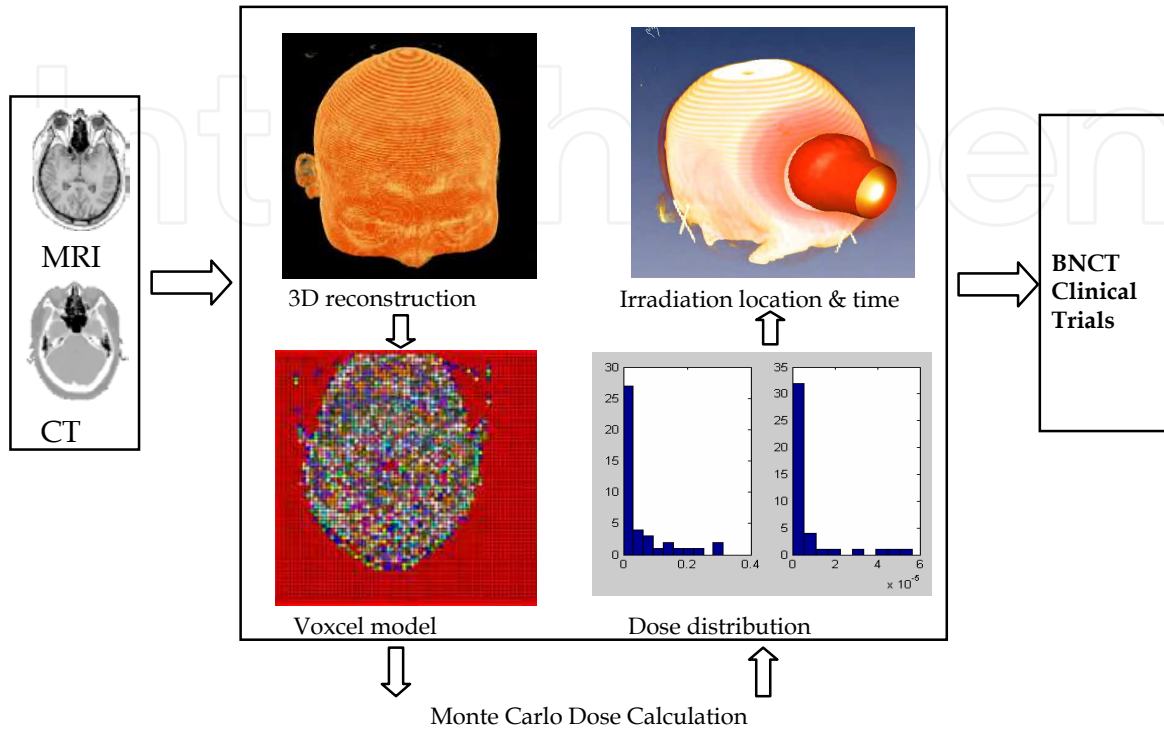


Fig. 1. Process of BNCT

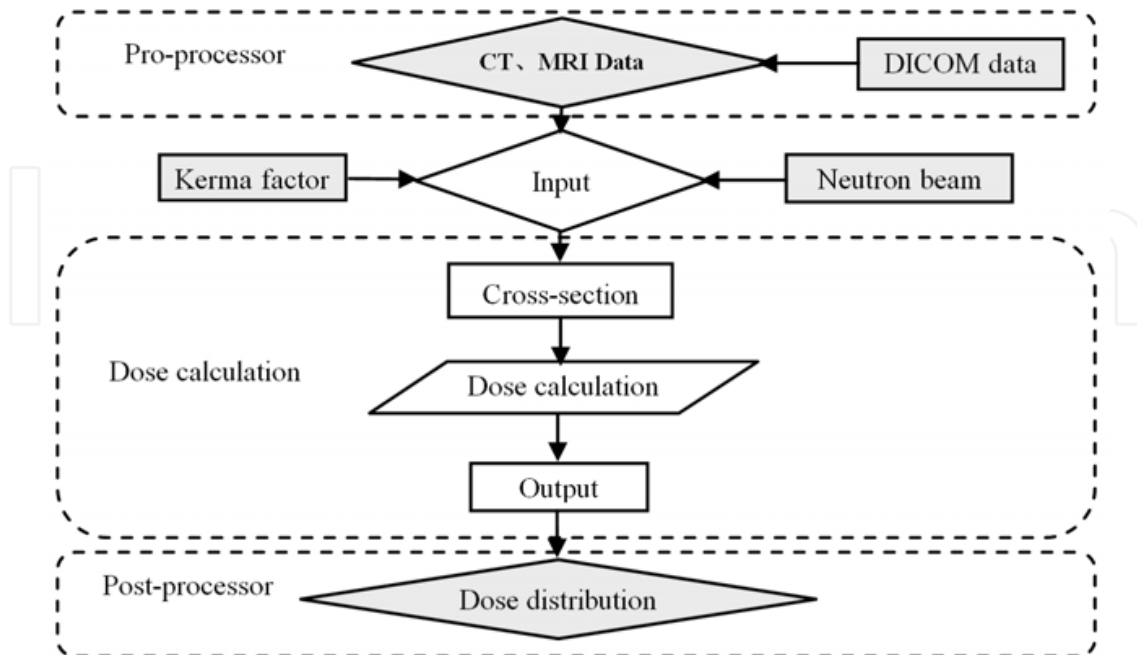


Fig. 2. Flow of BNCT TPS

Comparisons of BNCT TPSs have been limited in some scope. It is as far as know six TPSs, such as NCTPlan, MacNCTPlan (2002)<sup>[15]</sup>, JCDS (2004)<sup>[16]</sup>, BNCT-rtpe, SERA (2000)<sup>[17]</sup> and MCDB (2007)<sup>[18]</sup>, have been used in the clinical trials, where the Idaho National Energy and Engineering Laboratory's SERA and Harvard-MIT's MacNCTPLAN are thought as the most valid.

### 3. Pro-processor and post-processor

#### 3.1 Setting up of calibration curve

MDP is the pro-processor and post-processor of MCDB TPS. With a set of CT numbers and related mass densities of real tissues the calibration curve can be built by dividing the CT scale into a few groups and making linear fit in each group. While CT number in Hounsfield Unit was first defined by Kouris et al (1982)<sup>[19]</sup> and can be calculated based on the energy spectrum of X-ray CT and the linear attenuation coefficient of the real tissues as a function of the photon energy. Uwe Schneider *et al* (1996)<sup>[20]</sup> developed the stoichiometric method to calculate the CT numbers of materials with their mass densities and chemical compositions known. In this paper the stoichiometric method is taken to acquire all the CT numbers of real tissues taken from ICRP (1975)<sup>[10]</sup>.

Usually the CT scale is divided into two segments, which ranges from -1000 to 100 and from 100 to 1500, respectively, to make two linear calibration curves. In figure 3 the solid line is the calibration curve based on a GE 9000 CT scanner and the dash line is based upon a Siemens somatom plus 4 CT scanner. The X-ray tube kilovoltage is at 120kVp during the scans for the two scanners. Final calibration curves from the two type CT scanners fit close to each other for CT numbers below 100. The maximum deviation is about 5% at upper CT region.

#### 3.2 Conversion of CT numbers to elemental weights

How to obtain the elemental weights for the CT based voxel phantoms is concerned here. Normally several thresholds values are chosen to divide the CT scale (-1000~1500) into a set of groups. Within each group, the CT numbers have the same elemental weights.

The distribution of CT numbers in Hounsfield unit from the CT image data of a man's head is shown in figure 4, on which some real tissues are marked. The following points of view are taken into consideration for the division of the CT scale. First, there will be more groups in regions with high proportion of CT numbers according to figure 4, by contraries, in the lower and upper CT regions there will be fewer groups. Secondly, the variation of the elemental weights, especially for calcium and phosphorus, whose weights have significant influence on the dose distribution of electron beams<sup>8</sup>, is concerned during selection of the threshold values. Thirdly, the final weights of elements for each CT group is approximately represented by that of the real tissues, whose CT numbers calculated with the stoichiometric method are about in the middle of the CT group (see figure 3 and 4). The CT scale is divided into 24 groups in this paper, which is far exceeded the numbers of groups either from DeMarco (1998)<sup>[6]</sup> or from Ma (2002)<sup>[8]</sup>, and each group correlates to a real tissue from ICRP publication (1975)<sup>[10]</sup>. Mass density distribution comes from the calibration curve based on GE 9000 (solid line in figure 4). A CT based voxel phantom can be generated easily by converting the CT numbers into mass densities and elemental weights voxel by voxel.

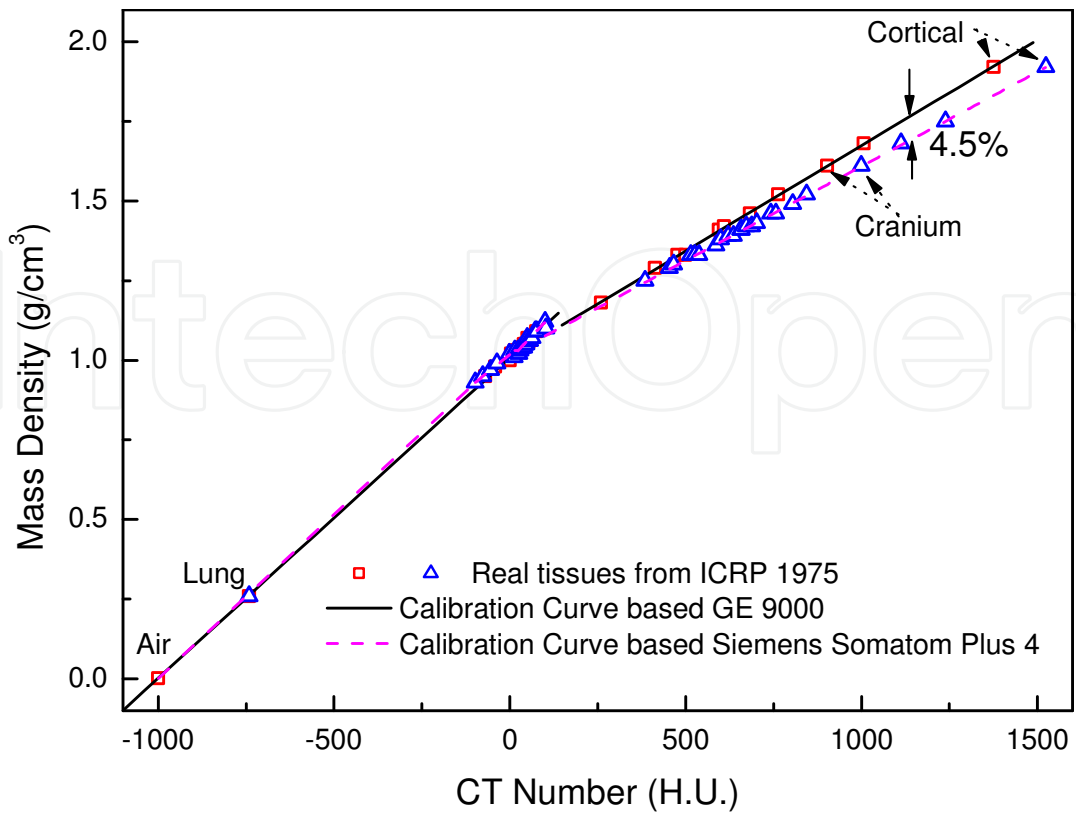


Fig. 3. Relationship between CT numbers and mass densities of real tissues

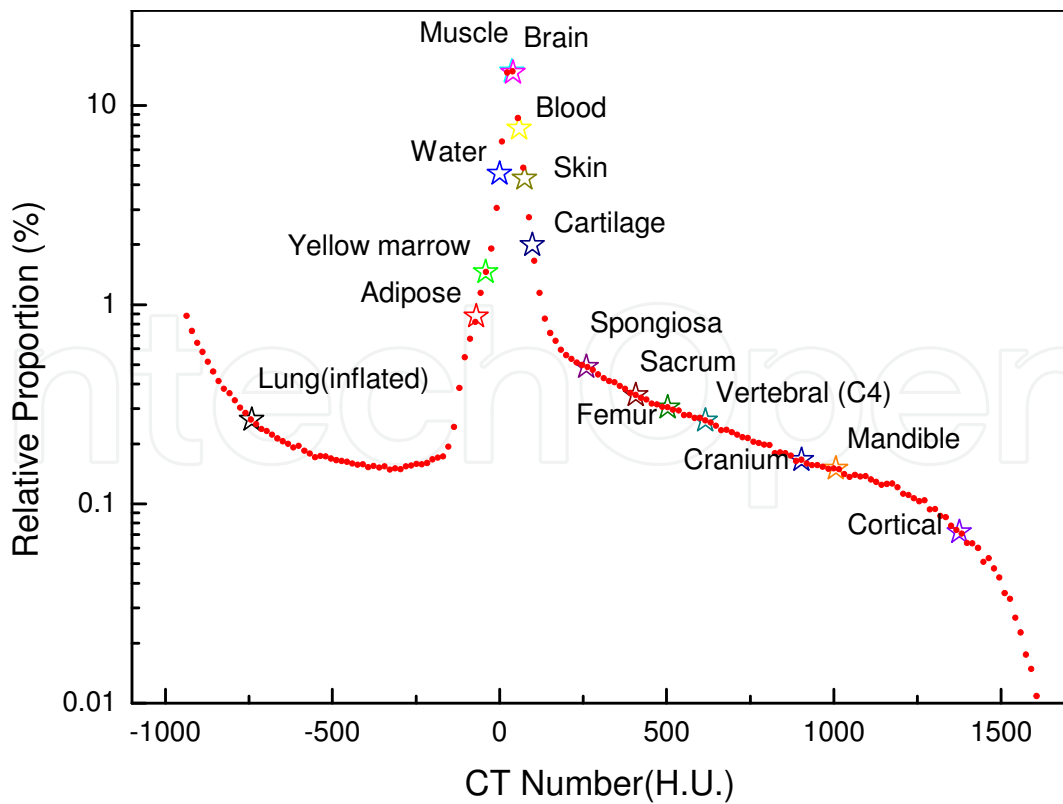


Fig. 4. Proportion of CT numbers for a human head

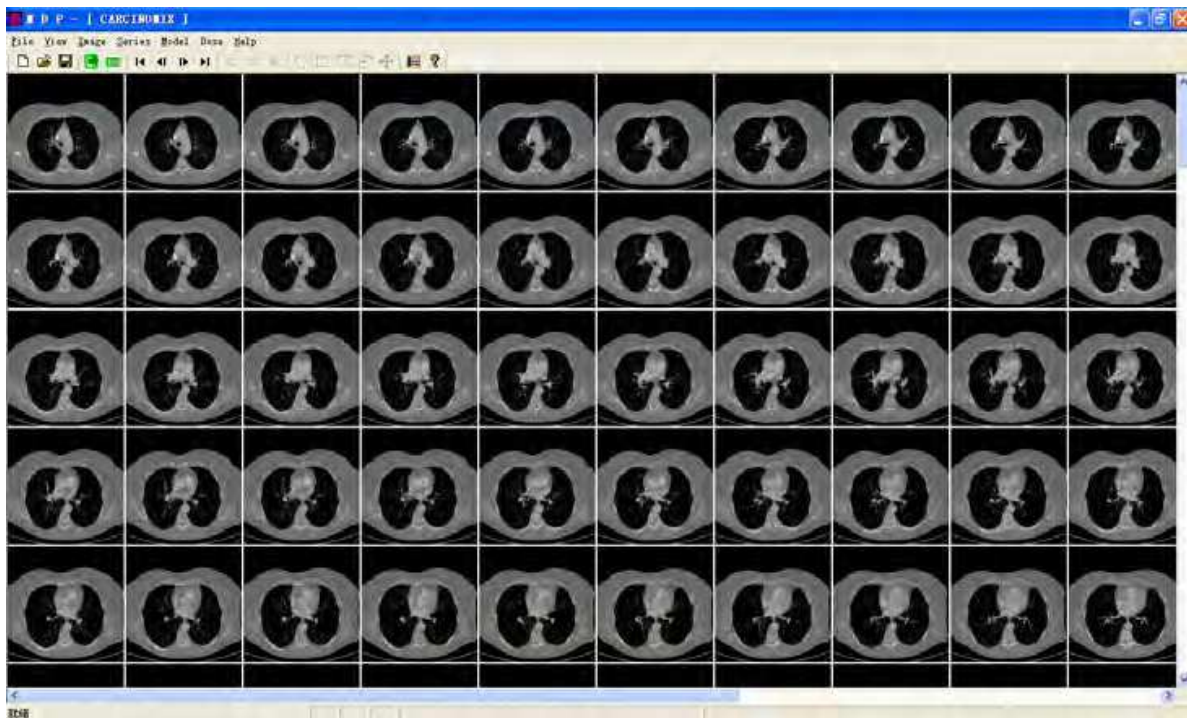


Fig. 5. Main interface of MDP

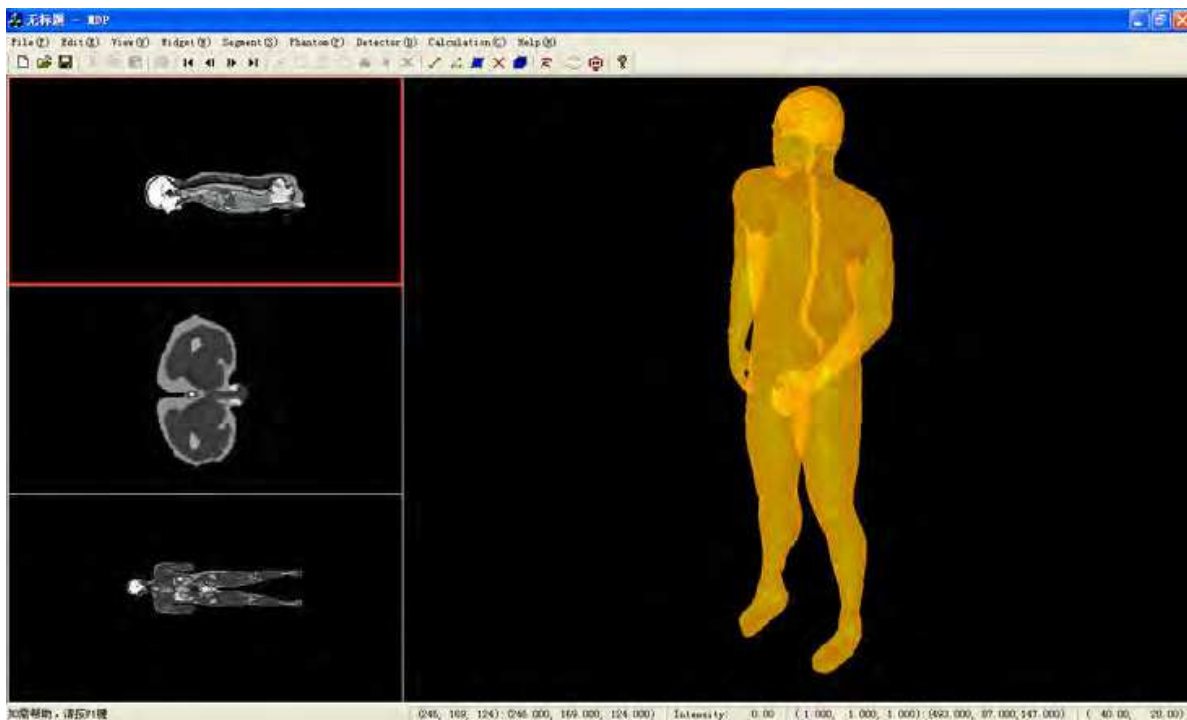
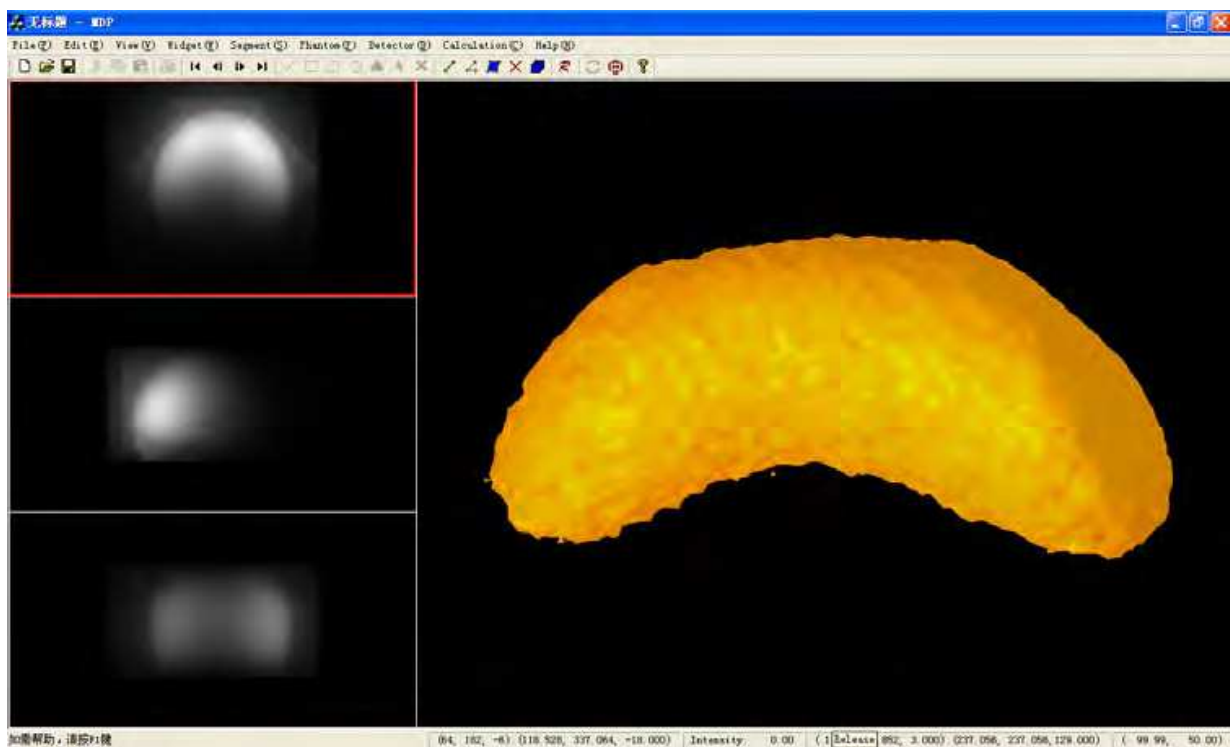
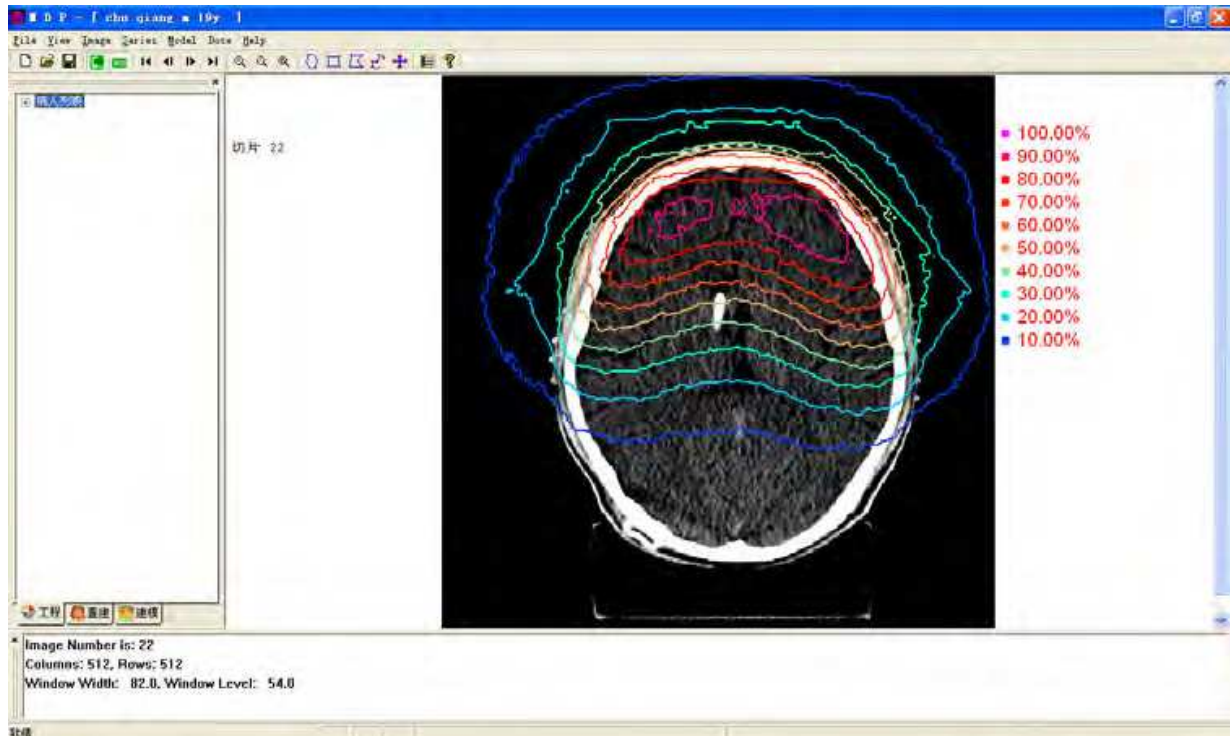


Fig. 6. Rendering of Zubal phantom

In MDP, the pro-processor processes volume data of a patient in DICOM or RAW format into an anthropomorphic phantom and translates it into an acceptable format for a Monte Carlo transport code. Of course, you can explore the patient’s medical images in client window with a self-defined window level and window width. Surface rendering function



based on MITK package supports extracting surface and rendering it for volume imaging data or volume dose data from dose calculator. Figure 6 shows the profile (Sagittal, Transverse, Coronal) of Zubal phantom and surface rendering results.



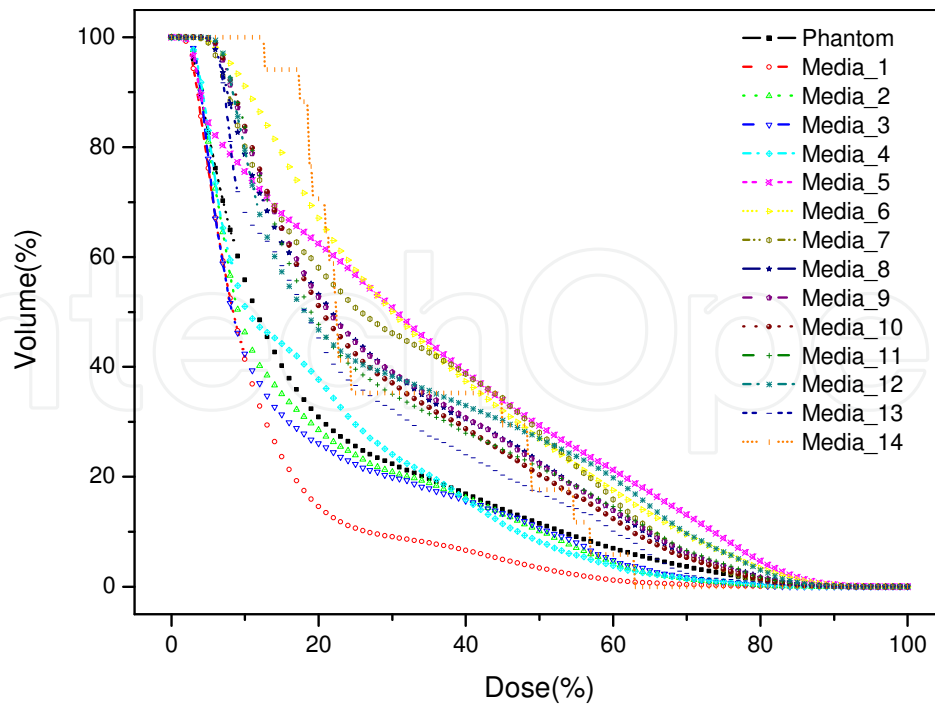


Fig. 7. Results processed by MDP, isoline, iso-surface and DVH

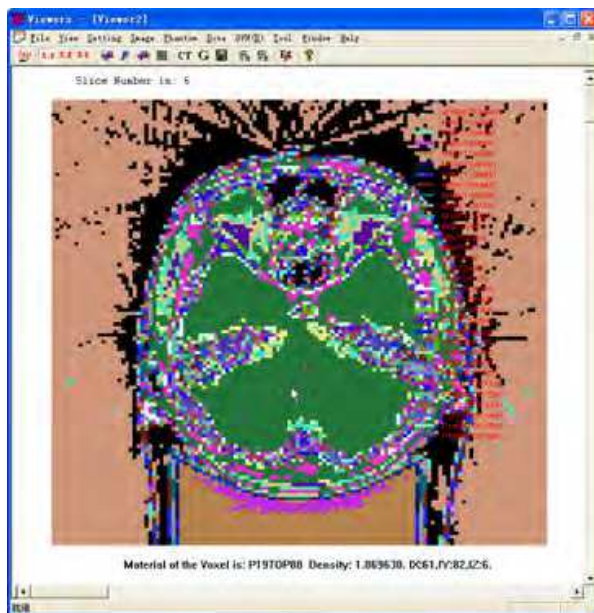


Fig. 8. Materials distribution for one slice

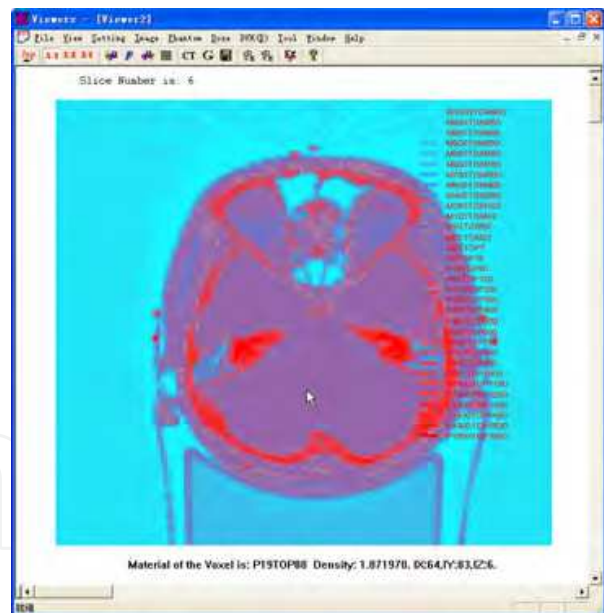


Fig. 9. Density distribution for one slice

At present, the dose calculation mainly represents general purpose Monte Carlo transport codes, such as MCNP<sup>[14]</sup>, EGS<sup>[21]</sup> and GEANT4<sup>[22]</sup>, etc. MCDB<sup>[18]</sup> can output an eligible input file for absorbed dose calculation. In case of BNCT, absorbed doses from thermal neutron, fast neutron and gamma will be scored separately. Also, volume dose related to 1ppm boron-10 and other interesting values will be scored.

The post-processor processes dose volume into all kinds of readable style, such as isoline, iso-surface and dose-volume-histogram, etc. An example is introduced to test the main

techniques that have been carried out in MCDB. We use a typical spectrum from a research reactor and an approximate angular profile (current/flux=0.65) as incident neutron source. The beam lights on the phantom from three direction (left, top, right) with weight of 0.3, 0.4 and 0.3 respectively. Isoline of one slice, iso-surface rendering of volume dose for 1ppm boron-10 and dose-volume-histogram for different medias are shown in figure 7 from left to right. Some figures for geometry viewer and dose viewer are listed as below.

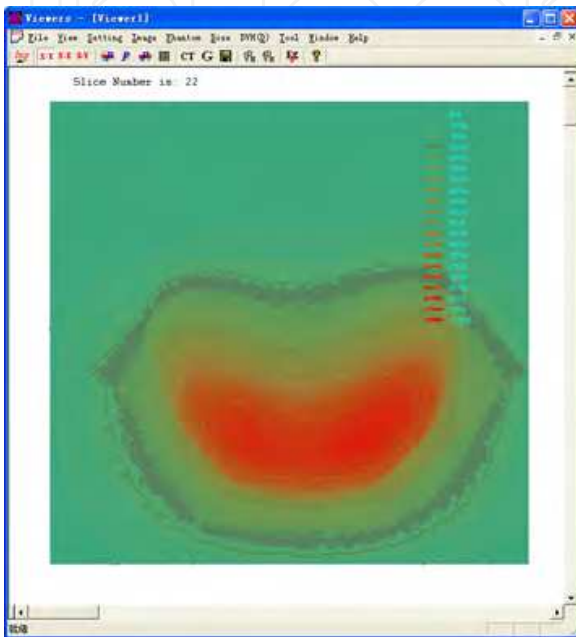


Fig. 10. Dose from thermal neutron distribution for one slice

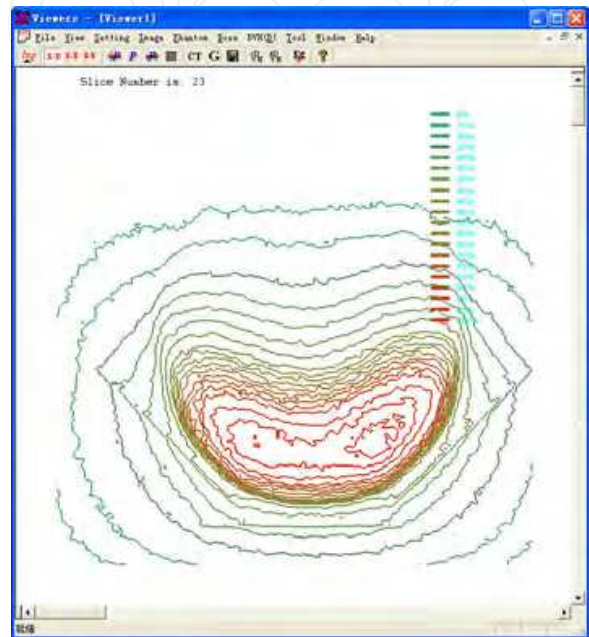


Fig. 11. Dose from 1ppm  $^{10}\text{B}$  distribution for one slice

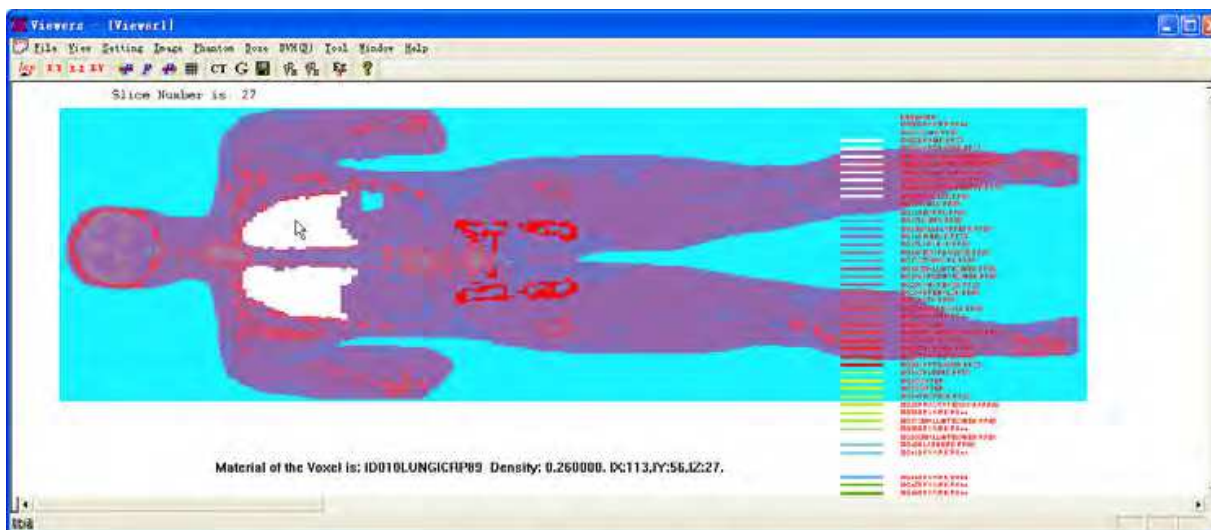


Fig. 12. Materials distribution (mouse clicked on lung) for one slice of Zubal Phantom (Geometry viewer of MDP)

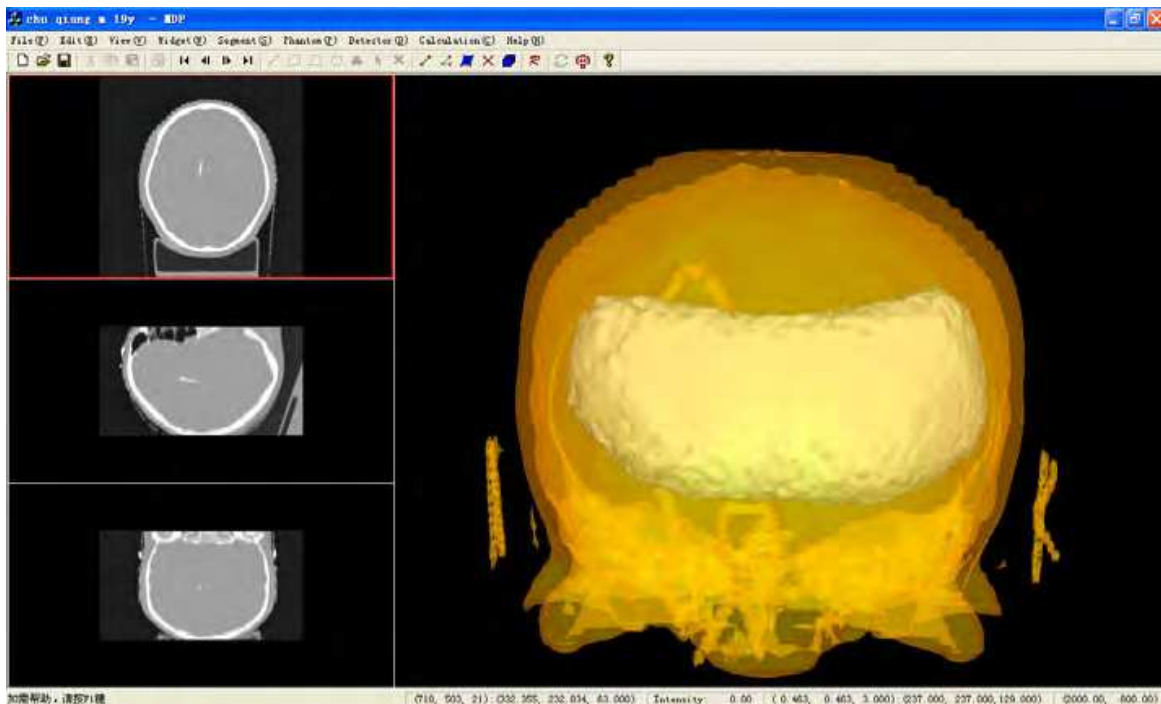


Fig. 13. Rendering results for dose from 1ppm  $^{10}\text{B}$  distribution with 60% iso-surface

#### 4. Reactor and neutron beam

Being the first step to start the BNCT studies, the neutron source has to be set up with the proper characteristics, which can create proper irradiation dose deposited at a desired position of the human body. The “proper” means the intensity of neutron flux or dose and the high ratio of useful flux or dose to harmful one requested by a reasonable treatment time. Thermal neutrons are the most wanted irradiation at tumor tissue in the BNCT treatment because of  $^{10}\text{B}(n,\alpha)$  reaction. However, the thermal neutron beam cannot penetrate tissues. The epithermal neutron beam is preferred to produce thermal neutrons at a certain depth inside tissues, because its average energy is higher than the thermal neutron beam. So, both thermal and epithermal neutron beams are necessary in the BNCT treatment.

To date, a number of facilities have been used for BNCT studies or clinical trials around the world. And they can be roughly classified as 3 types, general purpose research reactors using spectrum shifting and filtering or fission converters, accelerator-based neutron sources, and the dedicated single-purpose reactors.

Eight of such facilities are listed as examples, the epithermal facility at the BMRR of the Brookhaven National Laboratory in USA, the HFR at JRC in Pettern in the Netherlands, KURRI in Japan, the fission converter beam at MIT in USA, RA-6 facility in Bariloche in Argentina, epithermal beam at WSU in USA, the mixed mode beam at JRR-4 at JAEA in Japan, and the epithermal beam at FiR at VTT in Finland [23].

In this session, a newly designed dedicated single-purpose reactor will be introduced [24, 25]. The first In-Hospital Neutron Irradiator (IHNI) in the world was set up in China Institute of Atomic Energy (CIAE) in Beijing, China, in 2009. The IHNI with thermal power 30 kW is developed by Beijing Capture Technology Company (BCTC) which consists of GuoRun Construction Company, China Zhongyuan Engineering Coporation and China Institute of Atomic Energy.

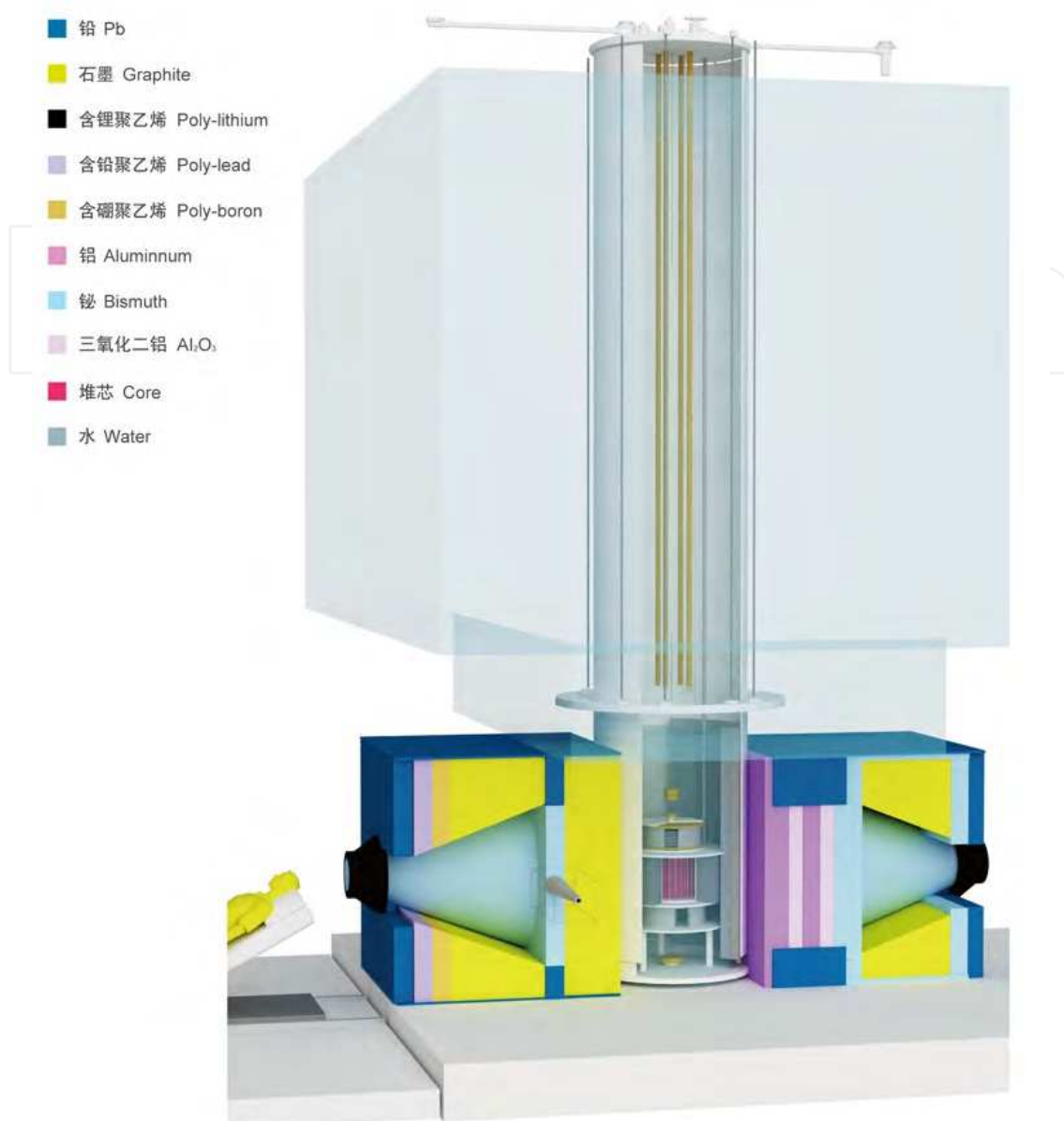


Fig. 14. In-hospital neutron irradiator (IHNI)

Based on modified Miniature Neutron Source Reactor (MNSR) techniques, the IHNI is an undermoderated reactor of pool-tank type with low enriched uranium (LEU) core, and can be installed on the basement floor of the main building or in an independent building. The IHNI uses  $\text{UO}_2$  with enrichment of 12.5%  $^{235}\text{U}$  as fuel, light water as coolant and moderator, and metallic beryllium as reflector. The IHNI has inherent safety with big negative temperature feedback, and its operation is done without any radioactive medium daily discharge to the environment. The fission heat produced by the reactor is removed by fully natural circulation cooling, and it includes no engineering operation facilities.

As a high efficiency neutron beam irradiation facility, the IHNI includes three beams, Epithermal neutron beam, Thermal neutron beam, and Blood-boron concentration measurement beam. The epithermal beam facility is equipped with the advanced energy spectrum regulator and high efficiency radiation shielding device. And the thermal beam Beam facility is equipped with thermalized neutron field and penumbra elimination device.

The last beam is designed for real time measurement of prompt gamma-ray neutron activation spectrometry analysis.

The IHNI also includes the complete medical treatment outfits for clinical trials and physics studies. The thermal neutron beam irradiation treatment room has full swivel bed for irradiation treatment of shallow focus while patients are in seating or laying positions and in-beam irradiation study of cells and small animals. The epithermal neutron beam irradiation treatment room has full swivel bed for irradiation treatment of deep focus while patients are in seating or laying positions. The treatment observation room is equipped with remote TV monitor, irradiation monitor and emergency treatment button. And the irradiation dosage detecting room is designed for gold foil activation detection, thermoluminescence brightness detection as well as blood-boron concentration gamma spectrometry analysis and assessment. The IHNI includes the boron compound batching and delivering room and computer software for treatment plan, too.

For treatment, the IHNI can provide  $\geq 1 \times 10^9$   $n_{\text{epi}}/\text{cm}^2 \text{ s}$  for deep focus irradiation of 30 minutes,  $\geq 2 \times 10^9$   $n_{\text{th}}/\text{cm}^2 \text{ s}$  for shallow focus irradiation up to four hours, and a homogeneous thermal neutron field with neutron fluence of  $\approx 10^{13}$   $\text{n}/\text{cm}^2$  for irradiation within beam facility. Meanwhile, the contamination irradiation dose rate is low at the beam port and in the air, in which the fast neutron contamination and the gamma ray contamination are smaller than  $6 \times 10^{-11} \text{cGy} \cdot \text{cm}^2/\text{n}$  and  $3 \times 10^{-11} \text{cGy} \cdot \text{cm}^2/\text{n}$ , respectively.

The construction cost of the IHNI is equal to the price of importing a set of advanced CT or MRI scanning diagnosis system (approximate Five Million Euros). Shown in figure 15, the

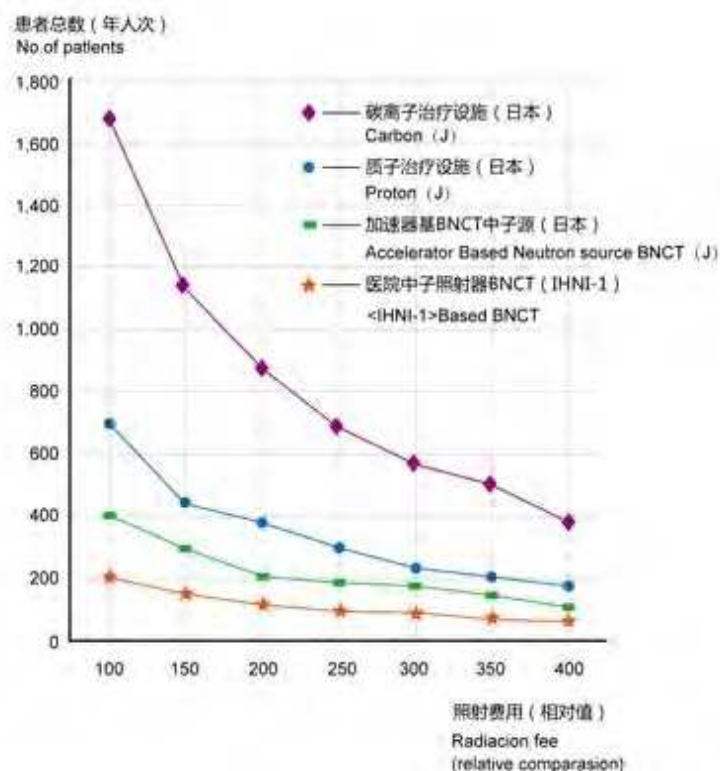


Fig. 15. Total cost of irradiation by IHNI

IHNI has the lowest operating cost comparing with the investment estimated by Japan to heavy ion beam irradiation treatment, proton beam treatment and the scheduled accelerator

neutron beam treatment on the basis of the providing irradiation treatment capacity for 200 patients per year. For these reasons, the IHNI is suitable for the clinical trials and studies in the large and medium-sized professional hospitals or comprehensive hospitals, the large and medium-sized medical colleges or medical research centers, and High efficiency pharmaceuticals research center or pharmaceutical factories.

## 5. Dose calculation

### 5.1 Physical dose distribution

The doses are primarily from four parts: (1) thermal neutrons; (2) boron-10; (3) fast neutrons; and (4) photons.

#### (1) Boron dose

The reaction of boron with neutron gives in equation (1). The  $^{10}\text{B}$  dose is primarily from  $^{10}\text{B}(n,\alpha)^7\text{Li}$  capture reaction with thermal neutron. The reaction releases the secondary gamma according to the probability of 94%. Since  $^{10}\text{B}$  has been isotope of choice due to the big thermal neutron capture cross-section of 3840 barns, a high Q-value of 2.79 MeV, the contribution of the boron dose is a big part of the total dose in spite of the boron consistence small (2002)<sup>[26]</sup>.

#### (2) Thermal neutron dose

The thermal neutron dose primarily arises from the  $^{14}\text{N}(n,p)^{12}\text{C}$  thermal neutron capture reaction, comprise 96% of the neutron kerma for ICRU-46 (1992)<sup>[27]</sup> brain tissue below 0.5 eV energy cutoff for thermal neutron.

#### (3) Fast neutron dose

The fast neutron dose tallies the full deposited energy from elastic neutron collision with hydrogen  $^1\text{H}(n,n)^1\text{H}$  and represents 90% of adult brain kerma between energies of ~600 eV to ~3 MeV. The remain dose about 4-8% is from the other neutron reactions, primarily with  $^{12}\text{C}$ ,  $^{31}\text{P}$  and  $^{16}\text{O}$  (2002)<sup>[26]</sup>.

#### (4) Photon dose

The photon dose component originates from two parts: (1) the contaminating photons from neutron beam incident on the target; and (2) the prompt gammas produced by the neutron capture in the target, primarily by  $^1\text{H}(n,\gamma)^1\text{H}$  reaction in tissue of brain.

#### (5) Kerma factor

The kerma (kinetic energy released in material) is a conversion factor from the flux to dose. The data is from ICRU-63 (2000)<sup>[28]</sup>, where the neutron is based on ENDF/B-VI library (1991)<sup>[29]</sup>. The key problem is how to treat the neutron of the energy lower 0.0253 eV.

#### (6) Flux

The flux in voxel  $j$  is obtained by Monte Carlo track length estimator.

$$\begin{cases} \phi(j, E) \approx \frac{S_0}{N} \sum_{n=1}^N \sum_m w_m^{(n)}(j, E) d_m^{(n)}(j), \\ w_m^{(n)}(j, E) = w_{m-1}^{(n)}(j, E) \left[ 1 - \Sigma_a^{(m-1)}(j, E) / \Sigma_t^{(m-1)}(j, E) \right] \end{cases} \quad (5)$$

Where  $S_0$  is the source intensity,  $N$  is the sample number (i.e. histories),  $w_m$  is a particle weight in  $m$ -th collision ( $w_0=1$ ),  $d_m$  is the track length in voxel  $j$ ,  $\Sigma_a$ ,  $\Sigma_t$  are the macroscopic absorption and total cross-section (1997)<sup>[14]</sup>.

## (7) Dose

When a particle passes through the voxel  $j$ , the dose tally of the voxel is:

$$dose(j) = \int \phi(j, E) \cdot kerma(j, E) dE / V(j) \quad (6)$$

where  $V(j)$  is the volume of the voxel  $j$ .

## 5.2 Some difficulties in dose calculation

Due to the complicated geometry and the neutron thermalization treatment, the Monte Carlo particle transport code with point-wise cross-sections is usually selected the first simulation tool. In the early, the general purpose MCNP Monte Carlo code (1997)<sup>[14]</sup> has been used for BNCT dose calculation, however the longer time consuming is the main drawback. In addition, MCNP is not for patient treatment planning. It is a general purpose, continuous energy, generalized geometry, time dependent, coupled neutron-photon-electron Monte Carlo transport code system. The flux and its response are obtained by an estimation of the track length. To obtain the track length, the intersection of a particle ray with the surface being traversed must be found. The collision point is sampled in each cell. The statistical data shows that the time percentage is over 60~70% in all transport computations. In addition, the initialization and tally times increase with decreasing voxel size. In article of Kiger et al.(2004)<sup>[30]</sup> showed the memory increase for variable size voxel, where the MCNP transport time increases in linear with decreasing of the voxel size. However, the tally and initialization times increase in exponent with decreasing of the voxel size. Tallies and their initialization time have a profound impact on the speed of voxel model calculations.

## 5.3 Voxel models

### (1) Analytical models

In Goorley et al.'s paper(2002)<sup>[26]</sup>, the Snyder head phantom model consists of three ellipses and four materials, where the inner region is the brain, the middle region is the skull and the outer region is skin. The area outside the head is air (see figure 16) . An ellipsoidal head phantom based on the Snyder model is used by the Harvard-MIT group for physical dosimetry of the two neutron beams at the MIT Research Reactor. The original Snyder head phantom consists of two ellipsoids, which divide the head into regions of cranium and adult brain. A third 5 mm thick shell representing skin has also been added. Equations (7)-(9), which locate the center of the head at the origin, specify these regions: the boundary between brain and skull:

$$\left(\frac{x}{6}\right)^2 + \left(\frac{y}{9}\right)^2 + \left(\frac{z-1}{6.5}\right)^2 = 1 \quad (7)$$

the boundary between skull and scalp:

$$\left(\frac{x}{6.8}\right)^2 + \left(\frac{y}{9.8}\right)^2 + \left(\frac{z}{8.3}\right)^2 = 1 \quad (8)$$

the boundary between scalp and air:



$$\left(\frac{x}{7.3}\right)^2 + \left(\frac{y}{10.3}\right)^2 + \left(\frac{z}{8.8}\right)^2 = 1 \quad (9)$$

The three different regions of the analytical modified Snyder head phantom are composed of adult whole brain, adult whole cranium, and adult skin materials, as defined by ICRU-46 (1992)<sup>[27]</sup> and listed in Table 1. Air, of composition described by Chadwick *et al.* surrounds the models. This geometry model is called in analytical model. It is used to test of treatment planning software.

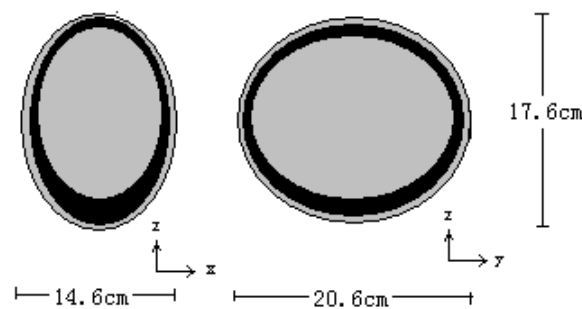


Fig. 16. Sections of the modified Snyder head phantom

Z	element	Air	Skeleton-Cranium	Adult whole brain	Adult skin
	$\rho$ (g/cm <sup>3</sup> )	0.00129	1.61	1.04	1.09
		3			
1	H	0	5.6	10.7	10
6	C	0.01	21.2	14.5	20.4
7	N	75.53	4	2.2	4.2
8	O	23.18	43.5	71.2	64.5
11	Na	0	0.1	0.2	0.2
12	Mg	0	0.2	0	0
15	P	0	8.1	0.4	0.1
16	S	0	0.3	0.2	0.2
17	Cl	0	0	0.3	0.3
19	K	0	0	0.3	0.1
20	Ca	1.28	17.6	0	0

Table 1. Material densities and compositions in mass percent.

## (2) Benchmark voxel models

For analytical model, three voxel models of 16, 8, 4mm are constructed (see figure 17). The majority of voxels contain only one of the four materials: air, skin, skull or brain. However, some cells in the boundary contain more than two of these basic materials. They are mixed in 10% increments and that result in an additional 282 kinds of new materials. Therefore, there are a total of 286 different materials. The analytical model uses ellipse geometries. The materials are composed of brain, skull and skin of an adult, as defined by ICRU-46 (1992)<sup>[27]</sup>.

The composition of air is described by Chadwick et al.(1999)<sup>[31]</sup>. Kerma data is from ICRU-63 (2000)<sup>[28]</sup>. At present, the Snyder head phantom analytical model and voxel models have been chosen as the benchmarks of BNCT. In general, the geometries of various organs are so complicated that they are difficult to describe by analytical geometry. Therefore, the analytical model represents a simplification of the actual physical geometry. In a clinical trial, CT and MRI image data, which are a group of discrete data, are used. It is then converted into a voxel model.

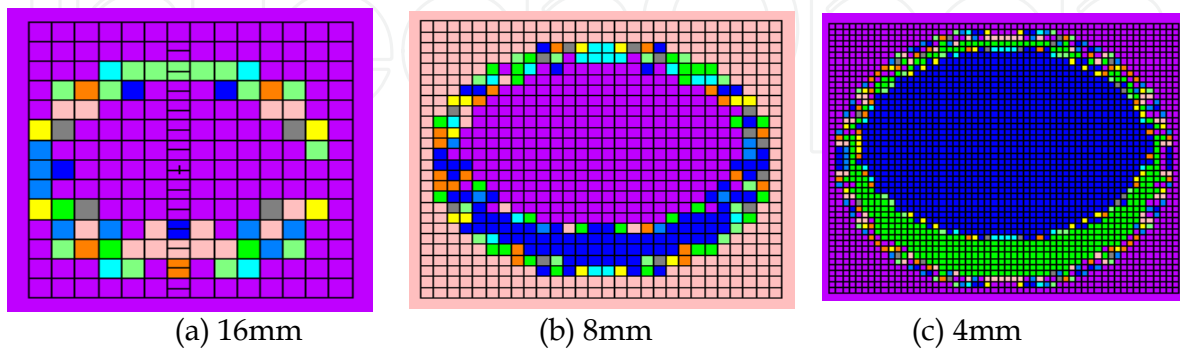


Fig. 17. Benchmark voxel models (mixture material)

### (3) Modified voxel models

The mixture material is very complicated in a boundary voxel of interface because the volume ratio of different materials is usually very difficult to be determined. A simple treatment takes the material and density of the voxel center point as the material and density of this voxel. It does not increase the new materials and keeps the basic four materials. The memory is obviously reduced. Of course, the center point method is valid if and only if the mass conservation satisfies. The mass maximal error of each tissue is usually less than 1%. Figure 18 gives the modified voxel models being produced by the center point method. Three modified voxel models are tested. The contents include mass, memory and computational time. The simulation tool is MCNP code. Table 2 shows the test results of 50 million histories. The results indicate that the mass conservation is good for the 4mm model, with a maximum error of 0.93%. However, the maximum mass errors are 4.48% and 19.79% for the 8mm and 16mm models, respectively. Both of these errors appear in the skin. Figure 19 shows the calculation result comparison of benchmark 4mm voxel model and modified 4mm voxel model. Almost same results are achieved. Too long computational time is main drawback no matter how 8mm or 4mm model.

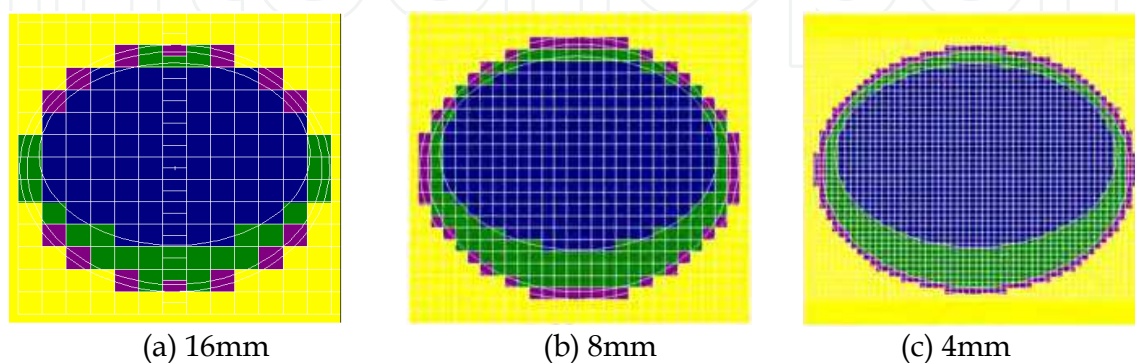


Fig. 18. Modified voxel and analytical models

mass (g) /model	brain error(%)	skull error(%)	skin error(%)	total mass error(%)	number of cubes	memory (MB)	cpu time (m)
Analytical	1529.1	1363.0	495.7	3387.8		6	326.01
Ben. 16mm	—	—	—	3394.7 (0.20)	2352	43	371.32
Ben. 8mm	—	—	—	3387.2 (-0.02)	16016	175	494.96
Ben. 4mm	—	—	—	3383.6 (-0.12)	94392	323	1208.60
Mod.16mm	1559.1 (1.96)	1266.2 (-7.10)	593.8 (19.79)	3419.1 (0.92)	2352	10	359.23
Mod. 8mm	1522.9 (-0.41)	1355.2 (-0.57)	517.9 (4.48)	3396.0 (0.24)	16016	37	489.36
Mod. 4mm	1528.0 (-0.07)	1370.4 (0.54)	491.1 (-0.93)	3389.5 (0.05)	94392	196	1206.81

Computer: Pentium IV 2.4 GHz PC machine and 50 million particles are simulated.

Table 2. Comparisons of mass, memory and computational time for different models

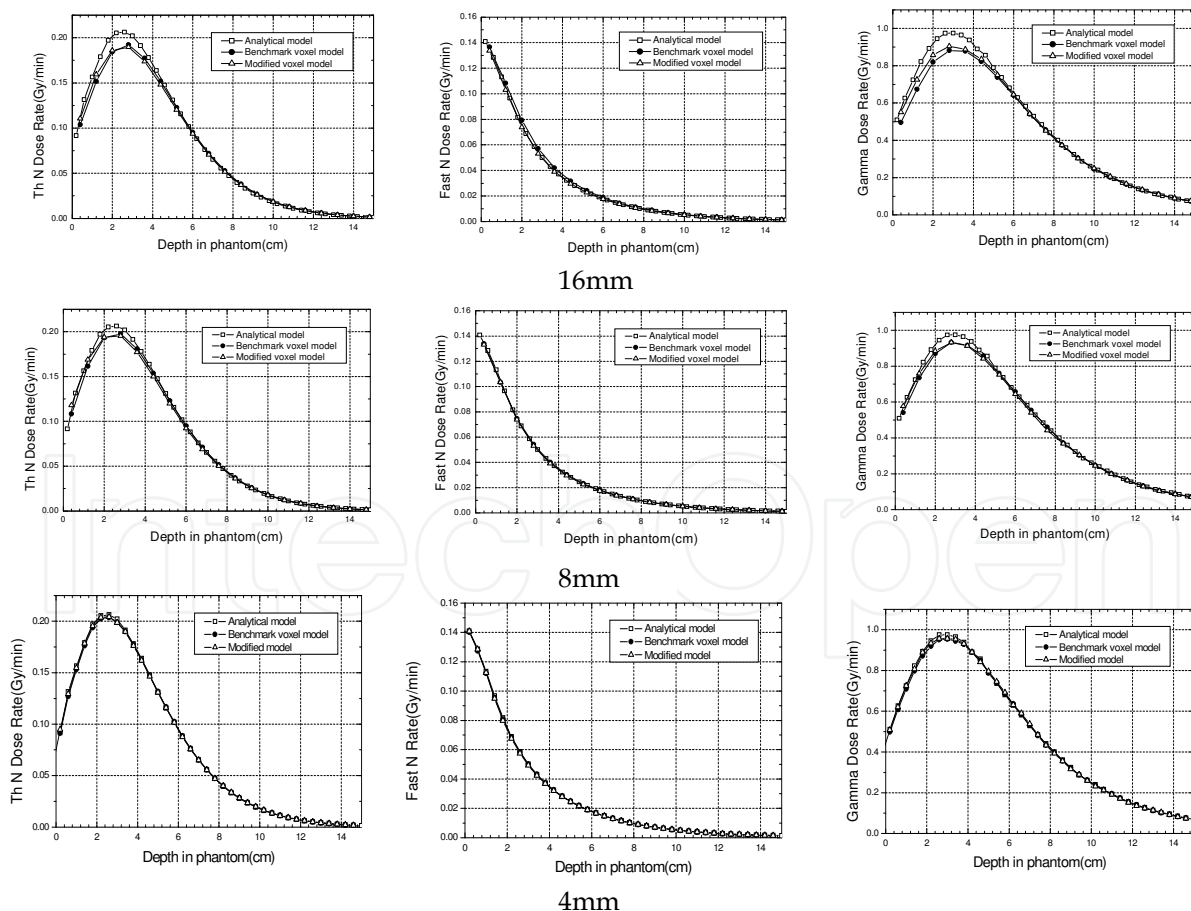


Fig. 19. Result comparisons of modified voxel, benchmark voxel and analytical models

## (4) Optimized voxel models

Take the dose distribution of the thermal neutron as an example, we can see that it firstly goes up before 2.5cm and then goes down till zero with the depth, and the peak value appears at about 2.5cm depth. After the 6cm depth, the dose becomes lower than that it gets in the skin. For a generic epithermal beam, the therapy effect is good before 6 cm depth, and 77.65% of the thermal neutron kerma rate is before 5.6 cm (it is defined as region I). 21.50% between 5.6cm and 12cm (it is defined as region II), only 0.85% left beyond 12cm (it is defined as region III) (see table 3). So the dose precision of the region I is a key. Table 2 shows that the dose errors of 8mm and 4mm voxel model are small, but a long computational time is taken. However, the computational time of 8mm voxel model is only a half of the time of 4mm voxel model. On the other hand, although some error exists for 16mm model, due to the dose contribution very small in region III, the 16mm voxel can be used in region III. So some optimized voxel models are designed. Figure 20 shows three combined voxel models. Figure 21 gives the comparison of thermal neutron calculation results and errors (fast neutron and photon similar case with thermal neutron). The big error appears in region III. Table 4 shows the comparison of the computational times. Table 5 shows the test of the mass. The results show that the 4+8mm combined voxel model almost keeps approach error of 4mm voxel model and the computational time is obviously shorter. But the computational time still exceeds 10 hours.

particles	depth (cm)		
	(I) 0-5.6	(II) 5.6-12.0	(III) 12.0--
thermal neutron	77.65%	21.50%	0.85%
fast neutron	85.53%	13.06%	1.29%
photon	63.26%	32.36%	4.00%

Table 3. Kerma rate of the analytical model

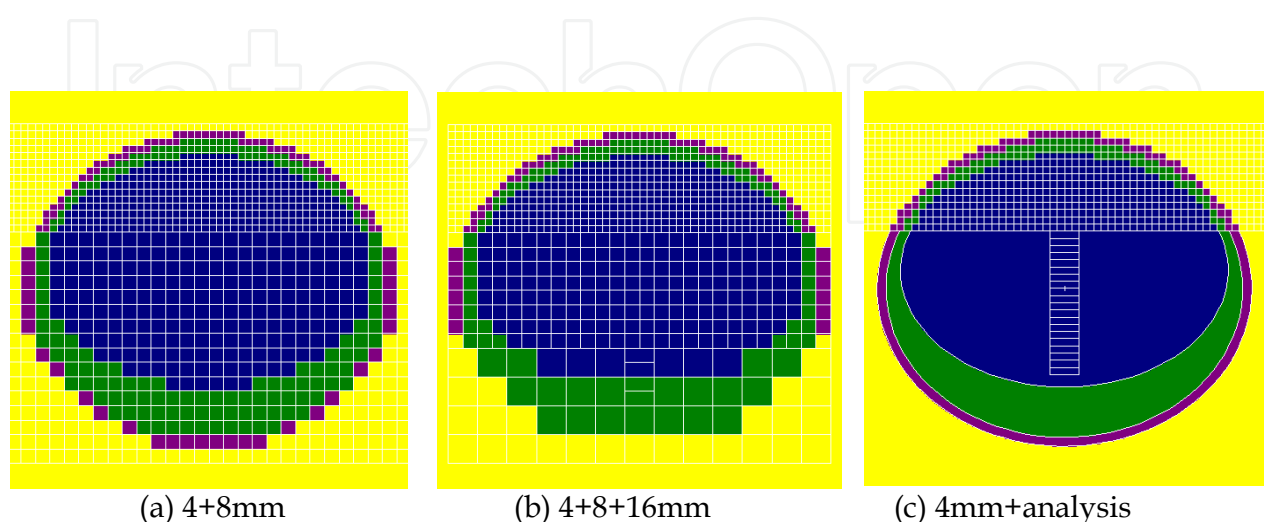


Fig. 20. The combined voxel models

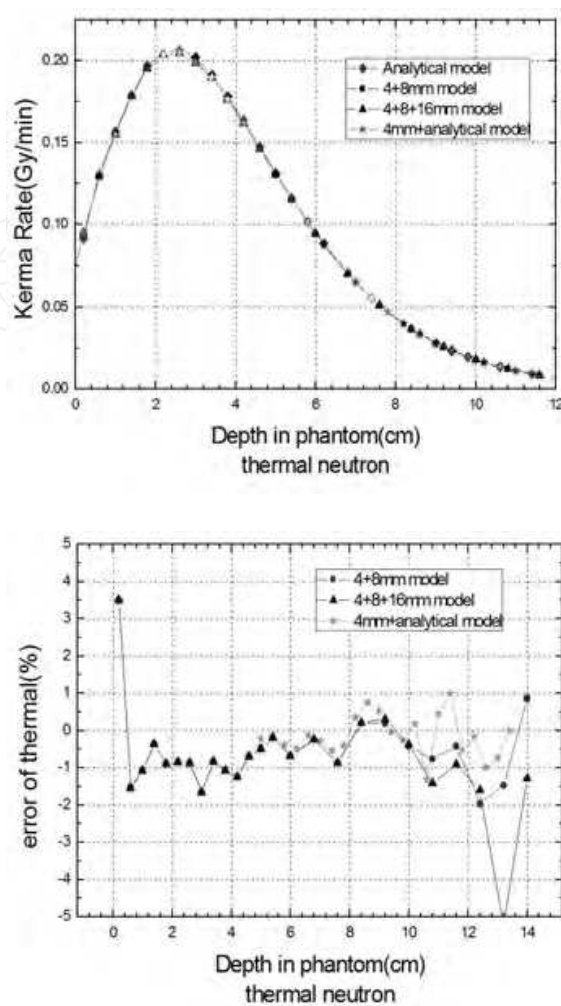


Fig. 21. Comparisons of doses and error of thermal neutron for combined voxel models

Model	Number of voxels	Memory (MB)	Time (min)	error (%)		
				thermal n	fast n	photon
8mm	16016	37	489.36	3.2025	1.6388	2.7715
4mm	94392	196	1208.60	0.8754	0.9612	1.1683
4+8mm	42560	89	693.88	0.9972	1.1508	1.7015
4+8+16mm	32292	70	639.58	1.0150	1.1690	1.7404
4mm+analytical	28104	71	622.67	0.8684	0.9813	1.1209

Table 4. Comparison of computational times and errors for combined models

Model	brain(g)	skull(g)	skin(g)	total(g)
analytical	1529.1	1363.0	495.7	3387.8
4+8mm	1524.2(-0.32)	1355.6(-0.54)	514.8(3.85)	3394.6(0.20)
4+8+16mm	1513.6(-1.01)	1398.5(2.60)	474.6(-4.26)	3386.7(-0.03)
4mm+analytical	1529.0(-0.01)	1363.3(0.02)	494.6(-0.22)	3386.8(-0.03)

Table 5. Tests of masses for combined models

## 5.4 Algorithms for dose calculation

### 5.4.1 Mesh tally matrix and material matrix

Two matrixes are used to tally the dose and store the material of each voxel. They are similar to the CT threshold matrix. The orders of the matrix are  $L \times M \times N$ , where  $L$ ,  $M$  and  $N$  are the mesh numbers in  $x$ ,  $y$  and  $z$  directions, respectively. Every element in the matrix expresses the dose or material of a voxel. When the particle ray passes through voxel, the voxel tally is performed. The total computational time does not increase in relation to the local cell tally because searching the tally cell is unnecessary. The mesh tally is a new tally in MCNP and it uses the simple planes to tally. The track length is easily calculated relative to the cell tally. The mesh tally matrix is a tally of MCDB. It is very simple and also uses the planes as well as arithmetical relationships.

### 5.4.2 Fast track length techniques

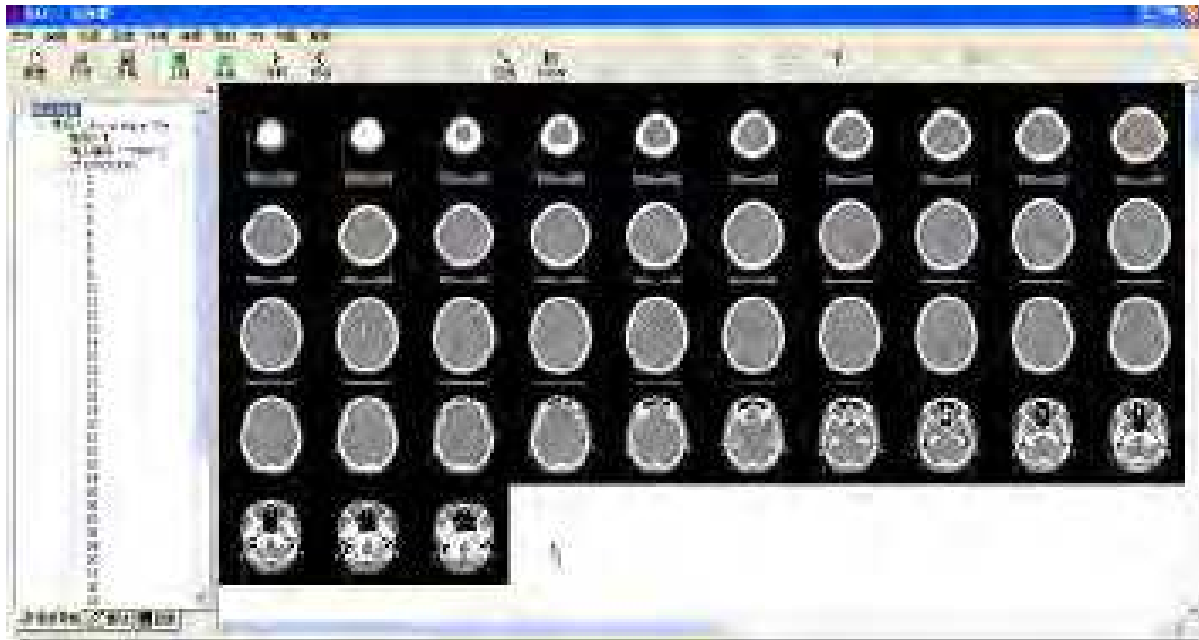
Firstly, each voxel is mapped on a unit cube. Then, the relationship among neighboring voxels is established. Each grid of every voxel is expressed as  $(i, j, k)$  in integer. It is also the voxel's ID. The interval range of the present voxel is defined by  $[i-1, i) \times [j-1, j) \times [k-1, k)$  (half open and half closed). Since each surface of every voxel belongs only to one side of another voxel, losing a particle can be avoided. The total number of neighbor voxels for the present voxel is twenty-seven, but only six voxels:  $[i \pm 1, j, k)$ ,  $[i, j \pm 1, k)$  and  $[i, j, k \pm 1)$  maintain the surface link relation. The other voxels only maintain the vertex link relation. When a ray passes through the vertex (i.e.  $f = 0$ ), the neighbor relation is valid. This case requires special treatment. When the material changes according to the IDs, the collision point is resampled.

For the voxel model, a cube is used and most of the voxels are of the same material. Once the direction of the ray is known, the ID of the next voxel and the track length are rapidly determined and calculation of the intersection is unnecessary. The details are described in reference [17,32].

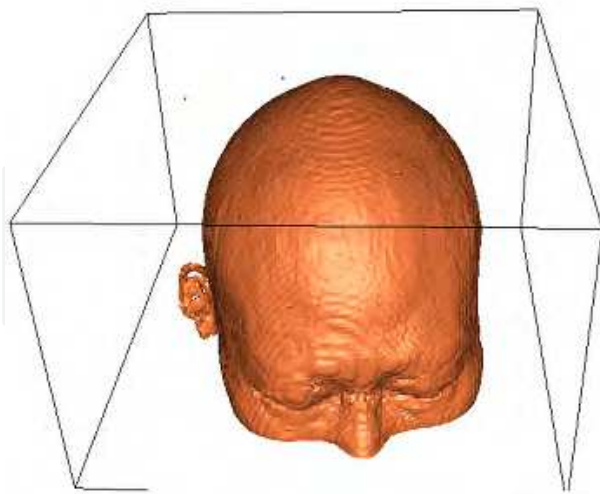
## 6. Example

This example is from a patient, which consists of 43 CT pictures (figure 22(a)). Firstly the 3-D reconstruction is done (figure 22(b)), then the two voxel models are designed, where one of model is CT8 which is consisted by  $8 \times 8$  pixels (the total cubes =  $64 \times 64 \times 43 = 176128$ , the size =  $0.3703 \times 0.3703 \times 0.3 \text{mm}^3$ ) and another model is CT4 which is consisted by  $4 \times 4$  pixels (the total cubes =  $128 \times 128 \times 43 = 704512$ , the size =  $0.1852 \times 0.1852 \times 0.3 \text{mm}^3$ , Fig.22(c)). The neutron beam is same as benchmark models. 10 million histories are simulated and all meshes are tallied. The figure 23 gives the comparison of the dose between MCDB and MCNP, where figure 23

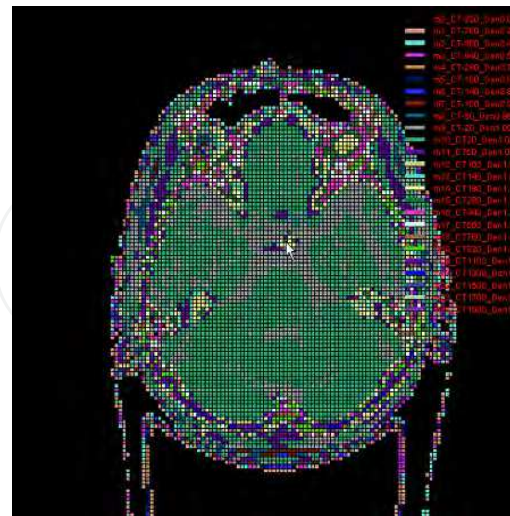
gives the dose distributions of the thermal neutron, fast neutron and secondary photon of each voxel. The almost same results of MCDB and MCNP are obtained. Table 6 shows the comparison of MCDB and MCNP in computing time. The figure 24 and 25 show the neutron dose surface and the photon dose surface. It is used to direct the irradiation.



(a)



(b)



(c)

Fig. 22. Cross section view of CT image and CT4 voxel model

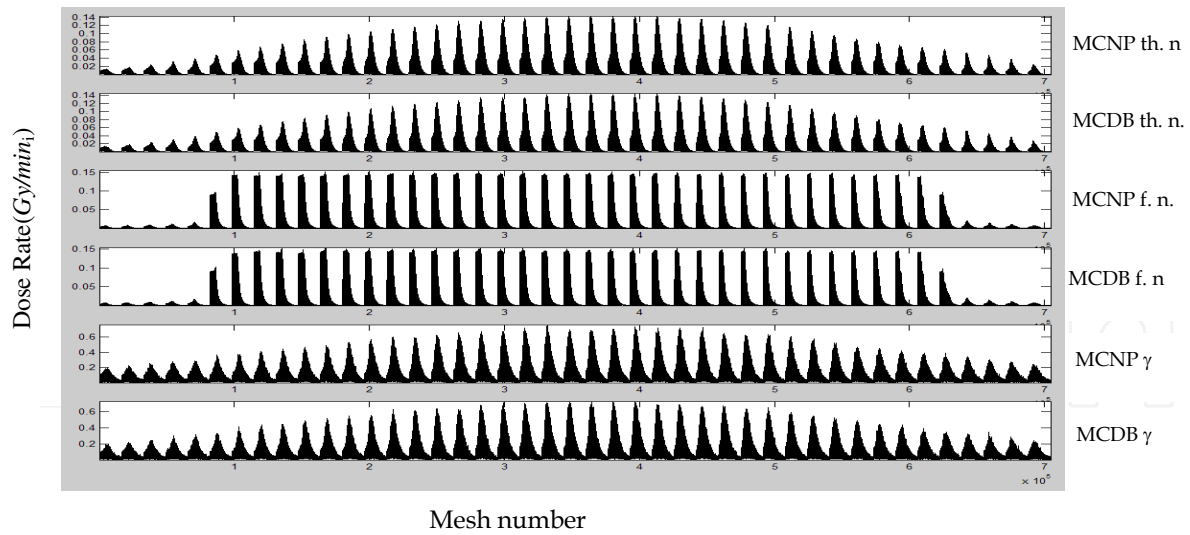


Fig. 23. Comparison of MCDB and MCNP result

model	voxel number	geometry	tally	code	time(m)	speedup
CT8	176128	lattice	mesh tally	MCNP	185.26	
		material Matrix	mesh tally matrix	MCDB	60.34	3.07
CT4	704512	lattice	mesh tally	MCNP	276.34	
		material Matrix	mesh tally matrix	MCDB	81.26	3.40

Computer: Pentium IV 3.0 GHz PC machine.

Table 6. Comparison of computing times based on the CT image model

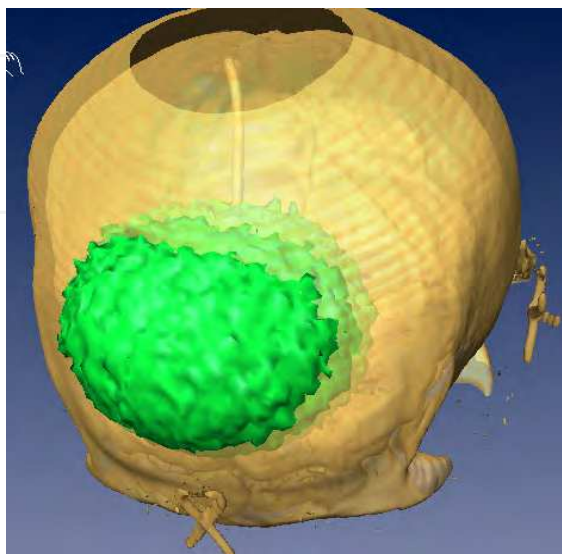


Fig. 24. Neutron dose surface



Fig. 25. Photon dose surface



## 7. Conclusions

The status of TPS recalls in this article. For a general TPS, the medical pro-processor, dose calculation and post-processor are included. In pro-processor, the basic data from CT and MRI DICOM image data is converted into the input file of voxel model for Monte Carlo dose calculation. The reactor device and neutron beam are an important part of BNCT. In the dose calculation, the several voxel models are constructed. For avoid to the difficulty of mixture material treatment in boundary interface, the modified voxel model is produced by the center point method. This method is valid for less than 4mm voxel models. At same time, the combined voxel models are design according to the dose varies with the depth. The test result is good and greatly reduces the computational time. However, these measures only partly decrease the simulation time if uses the general Monte Carlo MCNP code. It does not satisfy the clinical requirement. So some new algorithms, such as the fast track technique, material and tally matrix etc., are developed. These algorithms are written into the MCDB TPS. It makes the MCDB speed is fast about 3 times with respect to the MCNP. It basically satisfies the clinical requirement.

## 8. Acknowledgment

This research is supported by Capture Technology Ltd.. The authors also wish to thank Prof. Y. M. Zhou. This project is supported by CAEP fund (No. 2011A0103006).

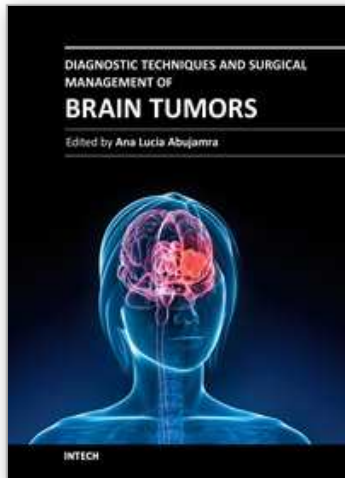
## 9. References

- [1] Rorer, A., Wambersie, G., Whitmore, et al. (2001). Current status of neutron capture therapy, *IAEA-TECDOC-1223*
- [2] Rolf F. Barth, Jeffrey A. Coderre, Vicente, M. G. H.(2006). Boron neutron Capture therapy, *Encycloped of Medical Devices and Instrumentation*, Second Edition, edited by John G. Webster
- [3] Snyder W S, et al.(1978). Estimates of absorbed fractions for monoenergetic photon sources uniformly distributed in various organs of a heterogeneous phantom MIRD Pamphlet no 5 (revised). *Society of Nuclear Medicine*, New York, USA
- [4] Zubal I G, et al.(1994). Computerized three-dimensional segmented human anatomy. *Med. Phys.* 21: 299
- [5] Kramer R, et al.(2003). All about MAX: a male adult voxel phantom for Monte Carlo calculations in radiation protection dosimetry. *Phys. Med. Biol.*, 48: 1239
- [6] DeMarco J J, et al.(1998). A CT based Monte Carlo simulation tool for dosimetry planning and analysis *Med. Phys.* 25: 1-11
- [7] WANG, L. et al.(2001). Monte Carlo Evaluation Of Tissue Inhomogeneity Effects In the Treatment of the Head And Neck. *Int. J. Radiation Oncology Biol. Phys.* 50: 1339
- [8] C-M Ma, et al.(2002). A Monte Carlo dose calculation tool for radiotherapy treatment planning. *Phys. Med. Biol.* 47: 1671
- [9] Schneider W, et al.(2000). Correlation between CT numbers and tissue parameters needed for Monte Carlo simulations of clinical dose distributions. *Phys. Med. Biol.* 45: 459

- [10] ICRP Publication 23 (1975). Report of the Task Group on Reference Man. *ICRP Publication 23*
- [11] ICRU-44(1989). Tissue Substitutes in Radiation Dosimetry and Measurement. *ICRU Reports 44*
- [12] Hatanaka, Y. and Nakagawa, Y.(1994). Clinical results of long-surviving brain tumor patients who underwent boron neutron capture therapy, *Int. J. Radiation Oncology Biol. phys.* ,1061
- [13] Zonta, A., Altier, S., Roveda, L., et al.(2008). Neutron Capture Therapy. *Proceedings of 13<sup>th</sup> International Congress on Neutron Capture Therapy*. Florence, Italy
- [14] Briesmeister, J. F., (Ed.) (1997). MCNP-A general Monte Carlo code for N-particle transport code, *LA-12625-M*
- [15] González, S., J., Santa Cruz, Kiger III, W., et al.(2002). NCTPlan, the New PC version of MacNCTPlan: Improvements and Verification of a BNCT Treatment Planning System, *Proceedings of the 10<sup>th</sup> International Congress on Neutron Capture Therapy for Cancer*, Essen, Germany
- [16] Kumada, H., Yamamoto, K., Matsumura, A., et al.(2004). Verification of the computational dosimetry system in JAERI(JCDS) for boron neutron capture therapy, *Phys. Med. Biol.* 49, 3353-3365
- [17] Seppälä, Kankaanranta, L., Serén, T., et al.(2000). BNCT\_RTPE and SERA Dose Planning Programs: Phantom and Patient Studies, *In Program and abstracts of 9<sup>th</sup> International Symposium on Neutron Capture Therapy for Cancer*, 175-176. ISNCT: Osaka
- [18] Li DENG, Gang LI, Tao YE, et al.(2007). MCDB Monte Carlo Code with Fast Track Technique and Mesh Tally Matrix for BNCT. *J. Nucl. Sci. Tech.* 44, 1518-1525
- [19] Kouris K, Spyrou N M and Jackson D F.(1982). *Imaging with Ionizing Radiations*. Surrey University Press, Glasgow
- [20] Schneider U, et al.(1996). The calibration of CT Hounsfield units for radiotherapy treatment planning. *Phys. Med. Biol.*, 41: 111
- [21] Kawrakow, I. and Rogers, D. W. O.(2000). The EGSnrc Code System: Monte Carlo simulation of electron and photon transport, Technical Report PIRS-701, National Research Council of Canada, Ottawa, Canada
- [22] [www.cern.ch/geant4](http://www.cern.ch/geant4); [www.ge.infn.it/geant4](http://www.ge.infn.it/geant4)
- [23] Auterinen, I., Serén, T., Anttila, K., et al.(2004). Measurement of free beam neutron spectra at eight BNCT facilities worldwide. *Appl. Radiat. Isot.* 61, 1021-1026 (2004).
- [24] Ke, G., Sun, Z., Lv, Z., et al.(2008). The study of Physics and Thermal Characteristics for In-hospital neutron irradiator (IHNI), *Proceedings of 13<sup>th</sup> International Congress on Neutron Capture Therapy*, 474, Florence, Italy
- [25] Li, Y., Xia, P. Zou, S. et al.(2008). The physics experimental study for In-hospital neutron irradiator, *Proceedings of 13<sup>th</sup> International Congress on Neutron Capture Therapy*, 474, Florence, Italy

- [26] Goorley, J.T., Kiger III, W.S., Zamenhof, R.G.(2002). Reference dosimetry calculations for neutron capture therapy with comparison of analytical and voxel models, *Med. Phys.*, 29(2), 145-156
- [27] ICRU-46(1992). Photon, Electron, Proton and Neutron Interaction Data for Body Tissues. International Commission on radiation Units and Measurements, *Bethesda, MD*
- [28] ICRU-63(2000). Nuclear data for neutron and proton radiotherapy and for radiation protection, *ICRU Report No. 63, International Commission on Radiation Units and Measurements, Bethesda, MD*
- [29] Cross Section Evaluation Working Group(1991). ENDF/B-VI Summary Documentation, *BNL-NCS-17541(ENDF-201)*, 4-th edition, National Nuclear Data Center, Brookhaven National Laboratory, Upton, NY
- [30] Kiger III, W.S., Albritton, J.R., Hochberg A.G., et al.(2004). Performance Enhancements of MCNP4B, MCNP5, and MCNPX for Monte Carlo Radiotherapy Planning Calculations in Lattice Geometries, *LA-UR-04-6972*
- [31] Chadwick, M., Barschall, H., Caswell, R., et al.(1999). A consistent set of neutron kerma coefficients from thermal to 150 MeV for biologically important materials, *Med. Phys.* 26, 974-991
- [32] Frandsen, M.W.(2001). Rapid Geometry Interrogation for Uniform Volume Element-Based BNCT Monte Carlo Particle Transport Simulation, *Proceedings of the Eighth International Symposium on Neutron Capture Therapy*, Plenum Press, New York

IntechOpen



## **Diagnostic Techniques and Surgical Management of Brain Tumors**

Edited by Dr. Ana Lucia Abujamra

ISBN 978-953-307-589-1

Hard cover, 544 pages

**Publisher** InTech

**Published online** 22, September, 2011

**Published in print edition** September, 2011

The focus of the book *Diagnostic Techniques and Surgical Management of Brain Tumors* is on describing the established and newly-arising techniques to diagnose central nervous system tumors, with a special focus on neuroimaging, followed by a discussion on the neurosurgical guidelines and techniques to manage and treat this disease. Each chapter in the *Diagnostic Techniques and Surgical Management of Brain Tumors* is authored by international experts with extensive experience in the areas covered.

### **How to reference**

In order to correctly reference this scholarly work, feel free to copy and paste the following:

Li Deng, Chaobin Chen, Tao Ye and Gang Li (2011). The Dosimetry Calculation for Boron Neutron Capture Therapy, *Diagnostic Techniques and Surgical Management of Brain Tumors*, Dr. Ana Lucia Abujamra (Ed.), ISBN: 978-953-307-589-1, InTech, Available from: <http://www.intechopen.com/books/diagnostic-techniques-and-surgical-management-of-brain-tumors/the-dosimetry-calculation-for-boron-neutron-capture-therapy>

**INTECH**  
open science | open minds

### **InTech Europe**

University Campus STeP Ri  
Slavka Krautzeka 83/A  
51000 Rijeka, Croatia  
Phone: +385 (51) 770 447  
Fax: +385 (51) 686 166  
[www.intechopen.com](http://www.intechopen.com)

### **InTech China**

Unit 405, Office Block, Hotel Equatorial Shanghai  
No.65, Yan An Road (West), Shanghai, 200040, China  
中国上海市延安西路65号上海国际贵都大饭店办公楼405单元  
Phone: +86-21-62489820  
Fax: +86-21-62489821

© 2011 The Author(s). Licensee IntechOpen. This chapter is distributed under the terms of the [Creative Commons Attribution-NonCommercial-ShareAlike-3.0 License](#), which permits use, distribution and reproduction for non-commercial purposes, provided the original is properly cited and derivative works building on this content are distributed under the same license.

IntechOpen

IntechOpen